Optical properties of the $Tl^0(1)$ center in KCl

L. F. Mollenauer, N. D. Vieira,* and L. Szeto
Bell Telephone Laboratories, Holmdel, New Jersey 07733
(Received 24 September 1982)

We report both experimental and theoretical studies of the $Tl^0(1)$ center in KCl, a center consisting of a neutral Tl atom perturbed by the field of an adjacent anion vacancy. Absorption bands peaking at 1040, 720, 550, and 340 nm are all shown to belong to the $Tl^0(1)$ center. The relatively weak ($f \lesssim 0.01$) bands at 1040 and 720 nm correspond to absorptions terminating on the crystal-field-split components of the $6^2P_{3/2}$ level, while the stronger band at 550 nm corresponds to transition to a state derived largely from $7^2S_{1/2}$. The sole luminescence band is the laser-active band having 1.6-μsec decay time and peaking at 1520 nm. The model presented here can account for the transition energies of the $6p$ manifold, including the Stokes shift between absorption (at 1040 nm) and luminescence, as well as the polarization properties and relative oscillator strengths of the 1040-, 720-, and 550-nm bands.

I. INTRODUCTION

Recently, two Tl atom defects in radiation damaged KCl:Tl have been discovered and analyzed by the use of electron spin resonance (ESR).[1] The new centers have been shown to consist of the neutral Tl atom strongly perturbed by the field of, respectively, one or two nearest-neighbor anion vacancies, and are accordingly named $Tl^0(1)$ and $Tl^0(2)$. At about the same time, a laser-active, Tl-associated center was discovered.[2] Significantly, its lowest-lying absorption (laser pump) band and emission (laser tuning) band always lay in the immediate neighborhood of the 1- and 1.5-μm regions, respectively, regardless of the particular alkali halide host. In this paper we shall show, on the basis of extensive optical evidence, that the laser-active centers are in fact $Tl^0(1)$ centers.

The electronic configuration of neutral Tl is $[Xe]4f^{14}5d^{10}6s^26p^1$; thus, in effect, one has to deal with a single p electron. The ground and first excited terms are $^2P_{1/2}$ and $^2P_{3/2}$, respectively, separated by a spin-orbit splitting of nearly 8000 cm^{-1}. (See Fig. 1.) In the neutral atom, of course, no electric dipole transitions connect these p-state terms, although strong ($f \sim 0.15$) transitions exist between each of these and the nearest lying even-parity ($7s$) states.

In the color center, the field of the surrounding ions can be analyzed as the superposition of terms of spherical, cubic, and odd symmetries, the latter due to an effective charge $+q_e$ of the defect. The odd term further splits (again, see Fig. 1) and alters the states of the $6p$ manifold. Of equal importance, it mixes in higher-lying even-parity states and thus allows for electric dipole transitions of modest strength within the $6p$ manifold; the one of these having lowest energy is the laser transition.

A segment of the absorption spectrum of a radiation damaged KCl:Tl crystal is shown in Fig. 2. We have been able to show, by way of a tagged-absorption technique (see Sec. III D), that the three

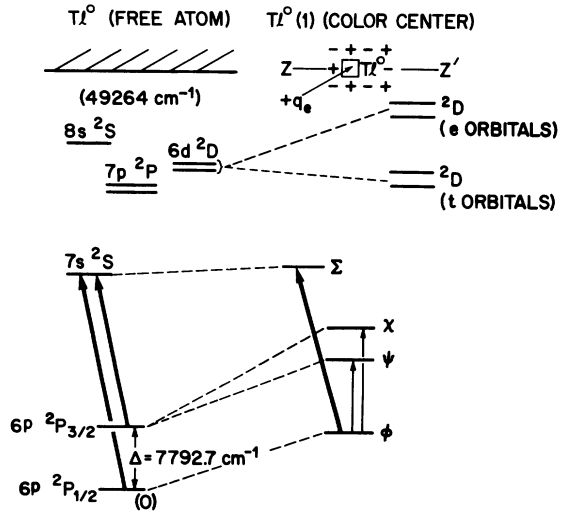

FIG. 1. Energy levels of atomic thallium (left) and of the $Tl^0(1)$ color center (right). The states labeled Φ, Ψ, and χ have largely $6p$ character, while the Σ state is derived largely from $7s$. The Φ and Ψ states contain significant admixture of the Σ state.

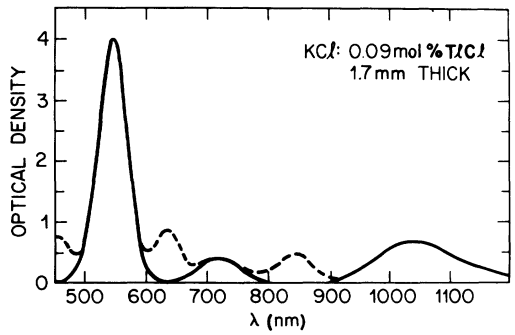

FIG. 2. Absorption spectrum of a radiation-damaged KCl:Tl crystal. The solid curve shows bands belonging to the $Tl^0(1)$ center; the full spectrum (dashed curve) contains bands belonging to other species.

bands shown by the solid curve all belong to the same center. Furthermore, as we shall show, the polarizations and oscillator strengths of all three transitions, and the energies of at least the lower two, make a good fit to predictions of a simple model based on the $Tl^0(1)$ configuration. In particular, the two weaker bands (peaking at 1040 and 720 nm) correspond to the transitions within the $6p$ manifold, brought about by the parity-breaking effect of the crystal field, while the much stronger band (at 550 nm) corresponds to transition to an even-parity state derived largely from the former $7s$ state.

It is important to compare the $Tl^0(1)$ center to the corresponding center with no perturbing defect. The latter, known as $Tl^0(0)$ in the notation of Goovaerts *et al.* (Ref. 1), has been studied experimentally by Delbecq and co-workers[3,4] and analyzed by Knox.[5] The fundamental absorption is a doublet, whose splitting and (very weak) strength increase rapidly with increasing temperature; the mean transition energy is just a bit lower (in KCl, by $\sim 7\%$) than the $^2P_{1/2} \rightarrow {}^2P_{3/2}$ spin-orbit splitting of the free atom. Both the splitting and the oscillator strength are induced by odd-parity phonon modes. Thus, in the $Tl^0(0)$ center, one has a dynamic version of the much larger, static effects described above for the $Tl^0(1)$ center.

The reduction in spin-orbit energy of the $Tl^0(0)$ center can probably be ascribed to a radial spreading of the wave function in response to the surrounding dielectric medium. A similar delocalization is to be expected in the $Tl^0(1)$ center. Thus, in the fitting of theory to experiment, it is justified to treat the spin-orbit splitting as an adjustable parameter; in fact, it would be unrealistic to expect the full free atom value to be represented in the color center.

Thus far, the discussion has been largely in terms of the effects of the odd field on states of the $6p$ manifold. However, crystal field terms of higher symmetry have important consequences for other aspects of the energy-level structure. In particular, the spherical term in the expansion of the crystal field looks like an inverted square well. This repulsive potential raises the energies of all states, thus bringing them closer to or into the continuum, but it has considerably greater effect on the radially compact states of the $6p$ manifold than on the more diffuse $7s$ and $6d$ states. (As can be seen from the radial distributions[6] plotted in Fig. 3, when in a $6p$ state the electron will with moderately high probability be found *within* the well, whereas when in the other states just mentioned, it will be found mostly *outside*.) It is undoubtedly this effect, more than any other, that is responsible for the reduction of the ground state to $7s$ energy separation from the ~ 3.3 eV found in the free atom to the ~ 2.3 eV found in the $Tl^0(1)$ center.

Delbecq *et al.* were also apparently able to estab-

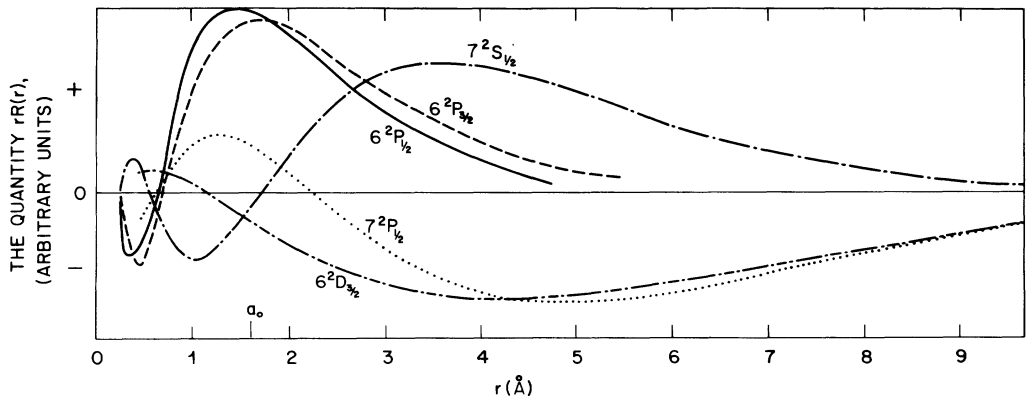

FIG. 3. The quantity $r\,R(r)$ for various states of atomic Tl, where $R(r)$ is the radial part of the wave function. The data for this figure are based on calculated wave functions. (See Ref. 6). The point $r = a_0$ represents the radius of the anion vacancy.

lish that the ground state of the $Tl^0(0)$ center lay ~ 1 eV below the edge of the conduction band, although details of the pertinent experimental evidence were not given.[7] Their conclusion is at least qualitatively consistent with the above-mentioned effect of the repulsive square well. However, it is hard to believe that the crystal field is strong enough to reduce the ionization energy of the $Tl^0(0)$ center [and by extension, of the $Tl^0(1)$ center] by more than a few eV (out of the ~ 6 eV required to ionize the free atom). Of course, in the $Tl^0(1)$ center, the attractive potential of the neighboring vacancy should somewhat deepen the ground-state energy with respect to that of the $Tl^0(0)$ center. Nevertheless, if the ground state of the $Tl^0(0)$ center is indeed as shallow as indicated in Ref. 7, then even in the $Tl^0(1)$ center, many of the higher-lying states, such as those of the $6d$ manifold, may well be degenerate with the continuum. One important effect of such degeneracy would be to bring about a compression in the energy spacings of the higher-lying states.

Although it has no effect on the splitting and separation of p states, the cubic field causes d-state terms to be split into groups of "t" and "e" orbitals,[8] separated by an energy of ~ 1 eV; the odd field can then further split these eigenstates of the cubic field. However, if as suggested above, the d states of the $Tl^0(1)$ center are degenerate with the continuum, the nature of those states and their splittings are undoubtedly complicated. Nevertheless, later on we shall show several absorption bands that may well represent transitions to states of the $6d$ manifold.

However, the major focus of this paper will be on the $6p$ manifold, its splittings and transitions. There are several reasons for this focus. First, the $6p$ manifold definitely corresponds to bound states, and its splittings should be determined only by the spin-orbit effect and the odd crystal field. Thus, the $6p$ manifold represents a set of levels apparently treatable by simple crystal-field theory, and may well represent the only levels of $Tl^0(1)$ so treatable. Hence, the fit between experiment and theory for this manifold represents the most accessible test of the $Tl^0(1)$ model. Second, the study was impelled by the desire to better understand the $Tl^0(1)$ center and analogous centers as laser materials; here again, the $6p$ manifold is of major (but not exclusive) importance.

It should be noted that to obtain best overall fit to our own (optical) data, we have had to choose crystal-field parameters slightly different from those selected in Ref. 1. However, to fit perfectly and simultaneously the optical and ESR data may require, as suggested in Ref. 1, an elaborate molecular-orbital treatment; such treatment is also beyond the scope of this paper.

II. THEORY

A. Crystal field and energies of the $6p$ manifold

The treatment and notation used here will follow closely that given in Goovaerts *et al.* (Ref. 1), except that it will be simplified to include only the $Tl^0(1)$ center. As in Fig. 1, let the z axis be the particular [100] axis passing through both the Tl nucleus and the center of the vacancy. The anion vacancy, in replacing the usual negative ion, is nominally equivalent to a positive unit electronic charge located at the center of the vacancy; however, to account for effects of lattice relaxation, both the effective charge and its exact location need to be adjustable. Therefore, let a charge $+q_e$ be located on the z axis at a distance r_0 from the Tl nucleus. To make it compatible with the atomic system the potential is expanded in a series of spherical harmonics centered at the nucleus. It is necessary to retain only the first two terms, as follows:

$$V_1(\vec{r})=q_e a(r)\cos\theta \tag{1a}$$

and

$$V_2(\vec{r})=q_e b(r)\tfrac{1}{2}(3\cos^2\theta-1)\,. \tag{1b}$$

Here $a(r)=r_</r_>^2$ and $b(r)=r_<^2/r_>^3$; $r_<$ and $r_>$ are the smaller and greater, respectively, of the distance r of the electron from the nucleus and of r_0.

To obtain the mixing of the $6p$ orbitals brought about by V_2, one diagonalizes the one-electron Hamiltonian

$$H=H_0-eV_2 \tag{2}$$

between the $6p$ orbitals. In matrix form, the Hamiltonian (2) is

$$\begin{array}{c|ccc} j,m_j & \frac{1}{2},\frac{1}{2} & \frac{3}{2},\frac{1}{2} & \frac{3}{2},\frac{3}{2} \\ \hline \frac{1}{2},\frac{1}{2} & \epsilon_{1/2} & \sqrt{2}\gamma & 0 \\ \frac{3}{2},\frac{1}{2} & \sqrt{2}\gamma & \epsilon_{3/2}-\gamma & 0 \\ \frac{3}{2},\frac{3}{2} & 0 & 0 & \epsilon_{3/2}+\gamma \end{array} \tag{3}$$

with a similar matrix for the states with $m_j<0$. In Eq. (3), $\epsilon_{1/2}$ and $\epsilon_{3/2}$ are the energies of the $6p_{1/2}$ and $6p_{3/2}$ states (of the free atom); thus $\epsilon_{3/2}-\epsilon_{1/2}=\Delta$, the spin-orbit splitting; the quantity $\gamma=-\frac{1}{5}q_e b$, where the factor $\frac{1}{5}$ derives from an integral over angular parts, and where the quantity b is a radial integral defined in Goovaerts *et al.* (Ref. 1). However, we do not distinguish between the on

and off diagonal terms ("b_1" and "b_2"), since they have nearly the same numerical values, and since, for present purposes, the difference can be accounted for by taking a slightly altered value for Δ. The energy eigenvalues resulting from diagonalization of matrix (3) are shown in Fig. 4, graphed as a function of the quantity γ/Δ.

B. Wave functions of the 6p manifold and of the nearest even-parity state

Corresponding to each of the three branches of Fig. 4 is a Kramer's doublet, which we call $\Phi^{\pm}$, $\Psi^{\pm}$, and $\chi^{\pm}$, respectively, from the lowest to highest energy; here the + and − signs refer to pseudo spin-up and spin-down states. To represent elementary orbital-spin product states, we use the shorthand notation $R_j^{nl}\,|\,l,m_l\rangle^{m_s}$ where $R_j^{nl}(r)$ represents the radial dependence of the wave function, and where the second factor represents the product of a spherical harmonic with a spin function. In terms of that notation, the eigenfunctions are as follows:

$$\Phi^+=\cos\theta R^{6p}_{1/2}(-\sqrt{1/3}\,|\,1,0\rangle^+ +\sqrt{2/3}\,|\,1,1\rangle^-) +\sin\theta R^{6p}_{3/2}(-\sqrt{2/3}\,|\,1,0\rangle^+ -\sqrt{1/3}\,|\,1,1\rangle^-)\,, \tag{4a}$$

$$\Phi^-=\cos\theta R^{6p}_{1/2}(\sqrt{1/3}\,|\,1,0\rangle^- -\sqrt{2/3}\,|\,1,-1\rangle^+) +\sin\theta R^{6p}_{3/2}(\sqrt{2/3}\,|\,1,0\rangle^- +1/\sqrt{3}\,|\,1,-1\rangle^+)\,, \tag{4b}$$

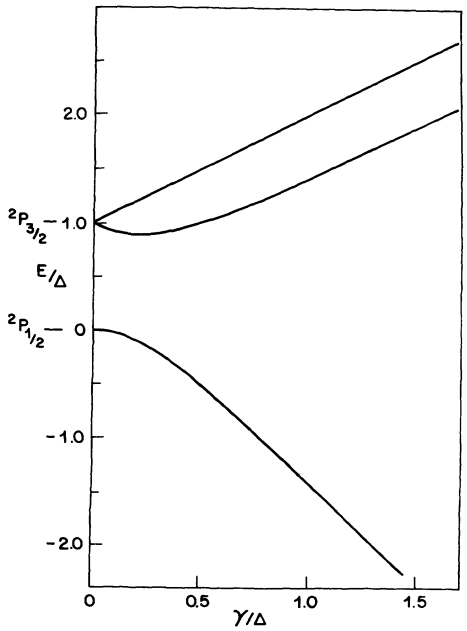

FIG. 4. Energies of the 6p manifold (measured in units of the spin-orbit splitting) versus the crystal-field strength parameter γ (measured in the same units).

$$\Psi^+=\cos\theta R^{6p}_{3/2}(\sqrt{2/3}\,|\,1,0\rangle^+ +1/\sqrt{3}\,|\,1,1\rangle^-) +\sin\theta R^{6p}_{1/2}(-1/\sqrt{3}\,|\,1,0\rangle^+ +\sqrt{2/3}\,|\,1,1\rangle^-)\,, \tag{4c}$$

$$\Psi^-=\cos\theta R^{6p}_{3/2}(\sqrt{2/3}\,|\,1,0\rangle^- +\sqrt{1/3}\,|\,1,-1\rangle^+) +\sin\theta R^{6p}_{1/2}(-\sqrt{1/3}\,|\,1,0\rangle^- +\sqrt{2/3}\,|\,1,-1\rangle^+)\,, \tag{4d}$$

$$\chi^+=R^{6p}_{3/2}\,|\,1,1\rangle^+\,, \tag{4e}$$

$$\chi^-=R^{6p}_{3/2}\,|\,1,1\rangle^-\,. \tag{4f}$$

In the above Eq. (4), θ is computed as

$$\theta=\tan^{-1}(-E_\Phi/\sqrt{2}\gamma)\,, \tag{5}$$

where E_Φ is the energy of the ground state $[E_\Phi(0)\equiv 0]$.

V_2 also brings about a mixing of even-parity states. Of particular interest here is the mixing of states of the 6d manifold with the 7s states. In principle, one can write down and diagonalize a Hamiltonian matrix for those states, just as was done above for states of the 6p manifold. However, certain pertinent quantities, such as the various radial integrals involved in the computation of matrix elements and the initial energy-level separations, are at best only vaguely known. Nevertheless, it can easily be shown that the only d state to be mixed in with the 7s state will be one of the "e" orbitals, namely, d_{z^2}. That orbital has a $|\,2,0\rangle$ angular dependence, and it can also be shown that it is mixed in with a negative coefficient. Therefore, the crystal-field state Σ, whose parentage is largely the atomic 7s state, will have the form:

$$\Sigma^{\pm}=\frac{1}{(1+\epsilon^2)^{1/2}}(R^{7s}\,|\,00\rangle^{\pm}-\epsilon R^{6d_{z^2}}\,|\,2,0\rangle^{\pm})\,. \tag{4g}$$

In the following, ϵ will be treated as an adjustable parameter ($\epsilon>0$).

The mixing in of even-parity states into the 6p manifold is brought about by V_1, and can be calculated by a simple perturbation treatment. For example, the coefficient of the Σ^+ state admixture into the Φ^+ state is given by the expression

$$C_{s+\Phi^+}=\frac{\langle\Sigma^+\,|\,V_1\,|\,\Phi^+\rangle}{E_s-E_\Phi}\,. \tag{6}$$

Similar expressions obtain for the other coefficients. Note that according to Eq. (6), the coefficient of Σ-state admixture will be directly proportional to the weighted sum of coefficients of the $|\,1,0\rangle$ terms in Φ, since V_1 has the angular dependence of a p_z state.

Thus for example, V_1 cannot bring about Σ-state admixture into the χ states, as these have no p_z component.

We have been able to obtain rather good agreement with the results of experiment by considering admixture of the Σ state only. There are several reasons for this success: First, the Σ state lies much closer to the $6p$ manifold than any of the other excited even-parity states, and second, in the color center, the oscillator strengths of transitions from the $6p$ manifold to those other states is low, relative to the $6p$-Σ transition strengths.

As will be shown in Sec. III B, the best overall fit to the optical data is obtained for $\gamma/\Delta=0.5$. Thus, from Eqs. (4) and (5), one can immediately calculate wave functions with specific coefficients. Furthermore, from those specific coefficients and from the Σ-$6p$ energy differences actually obtaining in the color center (see Fig. 2) one can also calculate the relative coefficients of Σ admixture. (For details, see Appendix A.) Thus, the ground ($\Phi^{\pm}$) and first excited ($\Psi^{\pm}$) state wave functions for the $Tl^0(1)$ center in its normal configuration in KCl become

$$\begin{aligned}\Phi^+ &= 0.819R^{6p}_{1/2}(-\sqrt{1/3}\,|\,1,0\rangle^+ + \sqrt{2/3}\,|\,1,1\rangle^-)\\ &\quad -0.574R^{6p}_{3/2}(\sqrt{2/3}\,|\,1,0\rangle^+ + \sqrt{1/3}\,|\,1,1\rangle^-)\\ &\quad -\beta\Sigma^+ ,\\ \Phi^- &= 0.819R^{6p}_{1/2}(\sqrt{1/3}\,|\,1,0\rangle^- - \sqrt{2/3}\,|\,1,-1\rangle^+)\\ &\quad +0.574R^{6p}_{3/2}(\sqrt{2/3}\,|\,1,0\rangle^- + \sqrt{1/3}\,|\,1,-1\rangle^+)\\ &\quad +\beta\Sigma^- ,\end{aligned} \tag{7a}$$

$$\begin{aligned}\Psi^+ &= 0.819R^{6p}_{3/2}(\sqrt{2/3}\,|\,1,0\rangle^+ + 1/\sqrt{3}\,|\,1,1\rangle^-)\\ &\quad +0.574R^{6p}_{1/2}(-\sqrt{1/3}\,|\,1,0\rangle^+ + \sqrt{2/3}\,|\,1,1\rangle^-)\\ &\quad +\beta\Sigma^+ ,\\ \Psi^- &= 0.819R^{6p}_{3/2}(\sqrt{2/3}\,|\,1,0\rangle^- + \sqrt{1/3}\,|\,1,-1\rangle^+)\\ &\quad -0.574R^{6p}_{1/2}(\sqrt{1/3}\,|\,1,0\rangle^- - \sqrt{2/3}\,|\,1,-1\rangle^+)\\ &\quad +\beta\Sigma^- .\end{aligned} \tag{7b}$$

[Note: It is only by accident that the relative amounts of Σ state admixed into the Φ and Ψ states are the same. This is due to the fact that the matrix elements of the crystal field just happen to be in proportion to the energy denominators in Eq. (6). See Appendix A.] Also note that the χ states remain as in Eqs. (4e) and (4f).

The absolute admixture of Σ state into the $6p$ manifold is not easy to calculate, since the overlap between each of the components of Σ ($7s$ and $6d$) on the one hand, and the $6p$ states on the other may be significantly different in the color center than in the free atom. Therefore we shall treat the quantity β in Eqs. (7a) and (7b) above as a parameter adjustable to empirically determined oscillator strengths.

However, we *are* now in a position to calculate several important quantities easily compared with experiment: (1) the polarization properties of transitions from the ground state to the Ψ, χ, and Σ states, and (2) the relative strengths of those transitions. The results of the calculations are summarized below in Table I. There σ_z, the cross section for light polarized parallel to the z axis, and σ_x, a similar quantity for light polarized (and propagating) normally to the z axis, are given relative to σ_0, the cross section for transition between pure $6^2P_{1/2}$ and $7^2S_{1/2}$ states.

In the following, we shall illustrate calculation of some of the cross sections given in Table I. First, note that for any transition between eigenstates of the crystal field, the net transition matrix element is the sum of matrix elements connecting the simple component atomic states. Each of the latter can be expressed as the product of two integrals, one involving only the radial dependences of the wave functions, the other involving only their angular dependences. The pertinent integrals are listed in Appendix B.

For example, consider the $\Phi\rightarrow\Psi$ transition. For light polarized along the z axis, the transition matrix elements are essentially $\langle\Psi^+\,|\,z\,|\,\Phi^+\rangle$ and $\langle\Psi^-\,|\,z\,|\,\Phi^-\rangle$. Therefore, the relative σ_z is given by

$$\begin{aligned}\frac{\sigma_z}{\sigma_0} &= \frac{2\beta^2}{1+\epsilon^2}\left[\begin{matrix}-0.819\sqrt{1/3}(1+\sqrt{0.8}\sqrt{4/5}\epsilon)-0.574\sqrt{2/3}(\sqrt{1.6}-\sqrt{1.37}\sqrt{4/5}\epsilon)\\ -0.819\sqrt{2/3}(\sqrt{1.6}+\sqrt{1.37}\sqrt{4/5}\epsilon)+0.574\sqrt{1/3}(1+\sqrt{0.80}\sqrt{4/5}\epsilon)\end{matrix}\right]^2\\ &= 4.99\frac{\beta^2}{1+\epsilon^2}(1+0.822\epsilon)^2 .\end{aligned} \tag{8a}$$

In the above, we have used the relative radial integrals derived from the experimentally determined oscillator strengths of atomic Tl, although of course, the algebraic signs must be taken from calculated wave functions. Also note that for transition between $P_{3/2}$ and D_{z^2} states, we have used the average radial integral for the transitions $6^2P_{1/2}\rightarrow 6^2D_{3/2}$ and $6^2P_{3/2}\rightarrow 6^2D_{5/2}$. The overall multiplication fac-

tor of 2 in Eq. (8a) stems from the fact that there are two z polarized transitions of equal strength: $\Phi^- \rightarrow \Psi^-$ and $\Phi^+ \rightarrow \Psi^+$.

For the right or left circularly polarized light propagating along the z axis, the pertinent matrix elements are $\langle \Psi^+ | (x+iy)/\sqrt{2} | \Phi^- \rangle$ and $\langle \Psi^- | (x-iy)/\sqrt{2} | \Phi^+ \rangle$, respectively. The relative absorption cross sections are then

$$\frac{\sigma_{x+iy}}{\sigma_0} = \frac{\beta^2}{1+\epsilon^2} \begin{bmatrix} 0.819\sqrt{2/3}(1-\sqrt{0.8}\sqrt{1/5}\epsilon) - 0.574\sqrt{1/3}(\sqrt{1.6}-\sqrt{1.37}\sqrt{1/5}\epsilon) \\ +0.819\sqrt{1/3}(\sqrt{1.6}-\sqrt{1.37}\sqrt{1/5}\epsilon) + 0.574\sqrt{2/3}(1-\sqrt{0.8}\sqrt{1/5}\epsilon) \end{bmatrix}^2$$

$$= 1.73\frac{\beta^2}{1+\epsilon^2}(1-0.748\epsilon)^2 \tag{8b}$$

with a similar expression for σ_{x-iy}/σ_0 leading to the same cross section. The quantity σ_x is then calculated as

$$\sigma_x = \tfrac{1}{2}(\sigma_{x+iy} + \sigma_{x-iy}) \, . \tag{9}$$

Following excitation to the Ψ state, the system relaxes to a new set of crystal-field parameters and wave functions significantly different from those cited above for the normal configuration. Let us designate quantities pertaining to the relaxed system with a subscript or superscript $*$. As we shall show in Sec. III B, the relaxation can be explained in terms of a shift of the crystal-field parameter γ such that $\gamma^*/\Delta \cong 0.25$. The new wave functions will have the same form as before; only the $\cos\theta$ and $\sin\theta$ factors and the coefficients of Σ-state admixture will change. From the value for γ^*/Δ just cited and from E^*_Φ taken from Fig. 3, Eq. (5) yields $\theta^* = 21.6°$. Thus for example, Φ^+_* is given by the expression:

$$\Phi^+_* = 0.930 R^{6p}_{1/2} \left[-\sqrt{1/3} \, | 1,0\rangle^+ + \sqrt{2/3} \, | 1,1\rangle^- \right]$$
$$-0.368 R^{6p}_{3/2} \left[\sqrt{2/3} \, | 1,0\rangle^+ + \sqrt{1/3} \, | 1,1\rangle^- \right]$$
$$-\beta^* \Sigma^+ \tag{10}$$

with similar changes for Φ^- and for $\Psi^\pm$. Additionally, the coefficient of Σ_*-state admixture for the $\Psi^\pm_*$ states becomes $0.865\beta^*$. (The energy denominators entering into calculation of the relative amounts of Σ_*-state admixture for the relaxed system are calculated from transition energies revealed in Sec. III C). The cross sections listed in Table I for the relaxed system were calculated from the relaxed wave function in the same manner as that indicated above for the normal configuration.

III. EXPERIMENTAL

A. Crystal growth and creation of the $Tl^0(1)$ centers

When the dopant is volatile, as is TlCl at the melting point of KCl, it is usual to grow crystals by the Bridgman technique in a closed ampoule. However, by using a tall, heated quartz cap on the crucible, we were able to produce crystals containing as much as ~ 1 mole % TlCl by the Czochralski method, with resultant high optical quality. Thallium concentration was measured by atomic absorption, using the addition method; samples for such analysis were taken from several places along each crystal.

Samples on the order of 1- to 2-mm thickness were sealed in aluminum foil and exposed (10–50 μA min/cm^2) to a 1.5-MeV electron beam, while cooled to ~ -130 °C by a stream of dry N_2 gas; this process mainly creates large ($\sim 1-5\times 10^{18}$/cm^3) densities of F centers. Then when the samples, at T ~ -30 °C, are exposed (from both sides, for times on the order of 10 min) to the light from a microscope lamp, several processes are set in motion: (1) the Tl^+ ions capture electrons from the ionized F centers [thereby becoming $Tl^0(0)$ centers] and (2) the resultant anion vacancies move through the crystal until each encounters and becomes bound, through Coulomb attraction, to a $Tl^0(0)$ center. [The anion vacancy has a positive and the $Tl^0(0)$ center a negative charge with respect to the lattice.] The temperature of ~ -30 °C represents a compromise: It is high enough to allow for reasonable mobility of the anion vacancies, yet low enough to prevent rapid dissociation of the $Tl^0(0)$ centers (required as an intermediate product, and unstable above 290 K). Several other routes to formation of the $Tl^0(1)$ centers are also possible: (1) Some $Tl^0(0)$ centers (along with Tl^{2+} centers) are formed directly during irradiation of the crystal. (2) Tl^+ ions with an adjacent anion vacancy are an alternate intermediate product; in that case, of course, electron capture completes formation of the $Tl^0(1)$ center. The conversion of Tl^+-F center pairs to $Tl^0(1)$ centers appears to be rather efficient [more than half the F centers destroyed can be used for $Tl^0(1)$ formation], although some other Tl-associated entities are formed, and there is also the possibility that an anion vacancy may simply annihilate its radiation damage counterpart.

TABLE I. Theoretical cross sections and polarization ratios.

Transition	$\Phi\rightarrow\Psi$	$\Phi^*\rightarrow\Psi^*$	$\Phi\rightarrow\chi$	$\Phi\rightarrow\Sigma$	$\Psi^*\rightarrow\Sigma^*$
$\frac{\sigma_z}{\sigma_0}$	$4.99\frac{\beta^2}{1+\epsilon^2}(1+0.822\epsilon)^2$	$4.89\frac{\beta_*^2}{1+\epsilon_*^2}(1.0.820\epsilon_*)^2$	0	$\frac{2.27}{1+\epsilon^2}(1+0.815\epsilon)^2$	$\frac{1.12}{1+\epsilon_*^2}(1+0.835\epsilon_*)^2$
$\frac{\sigma_x}{\sigma_0}$	$1.73\frac{\beta^2}{1+\epsilon^2}(1-0.40\epsilon)^2$	$1.79\frac{\beta_*^2}{1+\epsilon_*^2}(1-0.40\epsilon_*)^2$	$1.16\frac{\beta^2}{1+\epsilon^2}(1-0.413\epsilon)^2$	$\frac{0.062}{1+\epsilon^2}(1-1.45\epsilon)^2$	$\frac{0.96}{1+\epsilon_*^2}(1+0.408\epsilon_*)^2$
$\frac{\sigma_z}{\sigma_x}$	$2.88\left[\frac{1+0.822\epsilon}{1-0.40\epsilon}\right]^2$	$2.73\left[\frac{1+0.82\epsilon_*}{1-0.40\epsilon_*}\right]^2$	0	$36.6\left[\frac{1+0.815\epsilon}{1-1.45\epsilon}\right]^2$	$1.17\left[\frac{1+0.835\epsilon_*}{1-0.408\epsilon_*}\right]^2$

B. Transition energies, Stokes shift, and bandwidths

In this section we show that the various energy splittings and relative transition bandwidths of the $6p$ manifold can make an excellent fit to predictions of the crystal-field theory. The fit is obtained through judicious choice of two parameters: the crystal-field term (γ) and the spin-orbit splitting (Δ).

The two absorption ($\Phi\rightarrow\Psi$ and $\Phi\rightarrow\chi$) energies can be rather well fitted for γ/Δ in a certain range, through compensating adjustment in Δ. Therefore the fitting really begins with the Stokes shift (of the $\Phi\rightarrow\Psi$ transition), since the requirement to account for this shift places additional restraints on the choice of γ. The account is as follows: As indicated by Eq. (7a), the ground state is largely a p_z orbital, such that part of its electronic density distribution tends to occupy the vacancy (see Fig. 5). [The electronic density in the vacancy is enhanced by constructive interference on the vacancy side (destructive on the opposite side) between the s and p parts of the wave function. This interference effect may well account for at least part of the "delocalization" found by Goovaerts and co-workers (Ref. 1)]. Thus the surrounding positive ions are drawn in toward the vacancy center, thereby yielding a relatively large q_e for the center in its normal configuration. However, once the system has made transition to the Ψ state, the orbital is largely in the xy plane, and the charge density in the vacancy is correspondingly reduced. In this case the surrounding ions move outward through mutual repulsion, and q_e is made smaller. Thus it is at least plausible that the effective value of γ/Δ could be reduced, through such relaxation, to the considerably smaller value ($\gamma/\Delta\cong 0.25$) indicated in Fig. 5 for the luminescence. With this model, the crystal-field values indicated in Fig. 5, and $\Delta=6500\ \mathrm{cm}^{-1}$, the entire measured ($1.04\rightarrow 1.51\ \mu$m) Stokes shift can be accounted for.

The choice of γ/Δ values for the absorption and luminescence is also dictated by the fact that the emission bandwidth ($670\ \mathrm{cm}^{-1}$) is only about half the absorption bandwidth ($1360\ \mathrm{cm}^{-1}$) for the $\Phi\rightarrow\Psi$ transition at low temperature. One can imagine that the bandwidths are largely due to a breathing mode of the ions immediately surrounding the vacancy. Thus at low temperatures, q_e, and hence γ, would have the Gaussian probability distributions indicated in Fig. 5. The band shapes would then be given by the projections of those distributions on to the energy axis. By choosing points on the curve whose slopes are in a 2 :1 ratio, one then projects bandwidths in approximately the same ratio, as required to fit experiment.

Thus far, the adjustable parameters have been en-

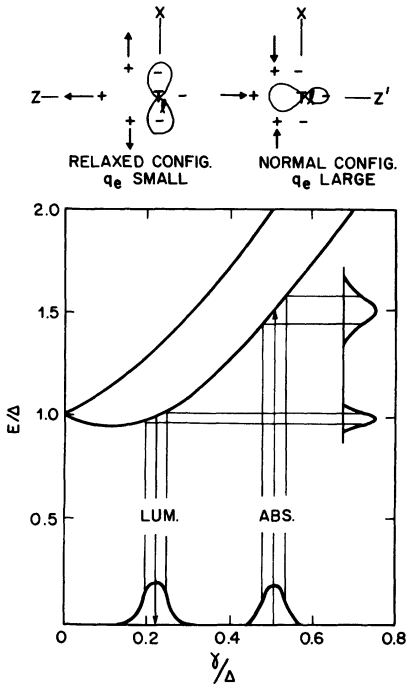

FIG. 5. Energies of the $\Phi \rightarrow \Psi$ and $\Phi \rightarrow \chi$ transitions as a function of the crystal-field energy parameter γ. Absorption takes place for $\gamma/\Delta = 0.5$ (normal configuration), while emission takes place for $\gamma/\Delta \sim 0.25$ (relaxed configuration). The change in γ/Δ can account for both the Stokes' shift and the relative bandwidths between absorption and emission.

tirely determined by requirements of the fundamental ($\Phi \rightarrow \Psi$) transition. However, the same parameter values yield a predicted energy for the $\Phi \rightarrow \chi$ transition in sufficiently good agreement with experiment (band peak at 720 nm) such that no further adjustment has been deemed necessary. The fit is summarized below in Table II.

It should be noted that the parameter values chosen for the fit are physically reasonable. For example, $\gamma = 0.5 \times 6500\ \text{cm}^{-1}$ (corresponding to the normal configuration) implies a value for q_e of $\sim +1$ electronic charge, and, of course, for the relaxed configuration, q_e has only about half that value. The best-fit value for Δ is $\sim \frac{5}{6}$ that of the free atom. As discussed in the Introduction, such reduction in Δ is to be expected by analogy with the $Tl^0(0)$ center. It is also at least qualitatively consistent with the delocalization required by ESR measurements of the hyperfine parameter.

TABLE II. Transition energies of the 6p manifold.

Transition	Predicted ΔE (cm^{-1})	Measured ΔE (cm^{-1})	Error (%)
$\Phi \rightarrow \chi$ (abs)	13 000	13 889	−6.4
$\Phi \rightarrow \Psi$ (abs)	9 750	9 615	+1.3
$\Psi \rightarrow \Phi$ (lum)	6 630	6 623	+0.1

The predicted ESR ground-state g factors are only in partial accord with the experimental results of Goovaerts *et al.* (Ref. 1). Corresponding to $\gamma/\Delta = 0.5$ one has $\theta = 35°$ [see Eq. (5)]; one can then read the g factors corresponding to the angle (and corresponding to pure p states) from Fig. 3 of Ref. 1. When the (only roughly known) s-state admixture is factored in, the predicted $g_{\|}$ becomes too large, while the predicted $g_{\perp}$ is still too small. Certainly, the fitting to the g factors given in Goovaerts *et al.* is considerably better. On the other hand, the parameters chosen there do not yield as good an overall fit to the optical data.

C. Measurement of the luminescence decay time

Thus far the only luminescence we have detected definitely associated with the $Tl^0(1)$ center is that of the fundamental ($\Psi \rightarrow \Phi$) transition. Measurement of the associated decay time τ_l, when combined with the quantum efficiency, immediately yields an absolute value for the oscillator strength of the luminescence. Furthermore, the oscillator strength of the associated absorption (not necessarily the same as that of the luminescence) can then be determined through measurement of saturation of the pumping.

To measure the decay times, we have used a technique especially suited to the infrared, where detectors combining high speed with high sensitivity are not readily available. The technique is indicated in Fig. 6. The beam from a cw pump laser (Nd:YAlG, $\lambda = 1.06\ \mu\text{m}$) was amplitude modulated [$I = I_0(1 + \epsilon \cos\omega t)$], and then allowed to impinge upon a sample that was optically thin at the pump wavelength. A spectrometer allowed transmitted

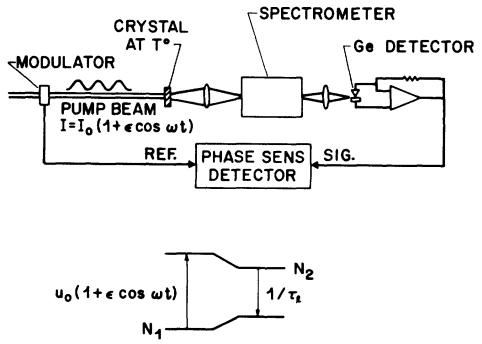

FIG. 6. Above: Apparatus for measurement of luminescence decay times by using a phase-shift technique. Below: The four-level pumping-luminescence cycle assumed in the technique.

pump light and luminescence to be separately detected, and the phases, Φ_l and Φ_p, of their respective modulation signals to be determined.

It can be shown that for a four-level system (see Fig. 6) where the nonradiative relaxation times τ_n and τ_n' are very short compared to the pump time u_0^{-1} and to the decay time τ_l, the difference in phase shifts, $\Phi=\Phi_l-\Phi_p$, is given by

$$\tan\Phi=\omega\tau_l \tag{11}$$

as long as $u_0\tau_l \ll 1$. Here the modulation index may have any value in the range $0\leq\epsilon\leq 1$. Thus, if the modulation frequency is chosen judiciously, Φ becomes an accurate measure of τ_l. (We have used $\omega/2\pi=50$ kHz, which suits the measured times, $\sim$ 1 μsec.) Note that the response characteristics of the detector do not enter into the determination of τ_l, since the phase shift contributed by the detector cancels in the calculation of Φ.

Using the above technique, we have measured τ_l as a function of temperature; the data are indicated in Fig. 7. Note that the decay time is nearly independent of temperature, except for the very highest part of the range. For a simple system such as the $Tl^0(1)$ center, it is hard to imagine a temperature-independent, nonradiative decay process. Therefore, we shall assume that the quantum efficiency, η, of the pumping-luminescence cycle is 100% for the lower part of the temperature range shown in Fig. 7. It then follows that the corresponding $\tau_l=1.6\pm0.05$ μsec is also the true radiative decay time τ_r.

From τ_r we can immediately determine the oscillator strength, f_{lum}, from the well-known formula:

$$f_{\text{lum}}=\frac{1}{8\pi^2}\frac{\lambda^2}{cr_0\tau_r}\frac{1}{n[(n^2+2)/3]^2}, \tag{12}$$

where c is the speed of light, r_0 the classical electron radius, λ the vacuum wavelength, and n the index of refraction of the host. (The term involving n corrects for the local field.) For $\tau_r=1.6$ μsec, $\lambda=1.5$ μm, and $n=1.47$, Eq. (11) yields $f_{\text{lum}}=0.0075$.

To determine the oscillator strength of the $(\Phi\rightarrow\Psi)$ absorption band, the measurements can be repeated, but this time with the pump beam carefully focused to a diffraction limited spot, and with intensity such that $u_0\tau_l$ is of order unity. It can be shown that, if the modulation index is small, say $\epsilon\lesssim 0.2$, and for a uniform intensity, the phase shift is given by the following:

$$\tan\Phi\cong\frac{\omega\tau_l}{1+u_0\tau_l}. \tag{13}$$

To account for the range of intensities present in the focused beam, the effects described by Eq. (12) must be integrated over a Gaussian intensity profile. Furthermore, one must account for the fact that the crystal contains several sets of centers, each having a different orientation of the center z axis with respect to the pumping field. Hence in general, each set will saturate at a different intensity level. We have not yet carried out the computer calculation required for an exact analysis of such a saturation experiment. However, preliminary measurements combined with "back of the envelope" analysis seem to indicate a value for f_{abs} at least several times greater than f_{lum}. Such a result is to be expected on the basis of the relaxation mechanism indicated in the preceding section. That is to say, f should scale approximately as β^2, and β should in turn increase directly with γ/Δ. Hence the $\sim$2 to 1 ratio of crystal-field parameters should yield an $\sim$4 times increase in f for the normal as opposed to the relaxed configurations. Fully analyzed saturation experiments will be reported on later.

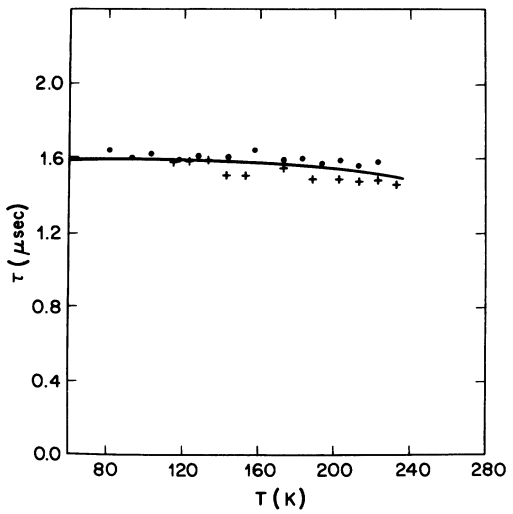

FIG. 7. Measured luminescence decay time τ_l, as a function of crystal temperature. The dots and crosses refer to data taken with two different samples.

D. Tagged absorption from the ground and first excited states

In this section we present evidence that the various transitions alluded to above do indeed belong to one and the same center. The principal experiment involves a technique[9] originally invented to measure excited-state absorption, although here the emphasis will be on the ability of that same technique to tag ground-state transitions. The method is shown in Fig. 8. A chopped laser beam (here at $\lambda=1.064$

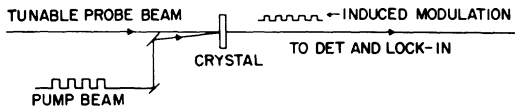

FIG. 8. Fundamental arrangement for the production of ground and first-excited-state absorption spectra tagged by selective optical pumping with a modulated beam.

μm) pumps the fundamental transition of the center under study; this pumping creates time-dependent populations in the ground and first-excited states of equal amplitude but of opposite phase. A tunable probe beam (light from a monochromator) is carefully focused on to the pumped spot. Modulation induced on the probe beam is then analyzed with aid of a phase-sensitive detector: signals "in phase" (actually lagging by $\tan^{-1}\omega t$) with the pump correspond to ground-state absorptions, and those "out of phase" correspond to absorption from the first excited state. A feedback loop is used to hold constant the time-averaged output of the detector. If, furthermore, the sample is optically thin for the transition under study, the resultant signals accurately represent the shapes and relative strengths of the various bands. But of greatest importance here, it can be *guaranteed* that the modulation signals all belong to the pumped center, and to no other species, provided that certain simple conditions are met: (1) The pumped band may not be seriously overlapped by bands of other species and (2) the pumped transition must be of lower energy than any transition of other species having significant concentration. The two conditions are required, of course, to avoid the pumping of other species, either directly, or through energy transfer.

In connection with the question of selectivity, it is helpful to use a chopping frequency high enough to yield a significant phase shift between the pump light and absorption signals. Then signals belonging to the desired species must all have that same phase shift, while signals of other species having presumably different decay times will exhibit distinctly different phase shifts. For the experiments to be described here, the modulation (chopping) frequency was 50 kHz, yielding $\Phi \cong 27°$ for signals from the $Tl^0(1)$ center.

For the crystals used in our tagging experiments, the $\Phi \rightarrow \Psi$ transition band (peaking at 1.04 μm) appears to meet fairly well both the conditions cited above. First, it is apparently overlapped only in its high-energy tail, while the pump wavelength used here (1.064 μm) lies on its long-wavelength side. (However, in samples not used here, but exhibiting a strong Tl_2^+ band following irradiation, a noticeable shoulder appears on the long-wavelength side of the 1.04-μm band.) Second, the two known bands of lower energy, i.e., the F_2^+ band at 1.38 μm and the Tl_2^+ band at 1.76 μm, were either reduced below the threshold of detectability (the F_2^+ band), or else have not been seen at all (the Tl_2^+ band), in the samples used.

Details of crystal and beam orientations were as follows: The sample was an optically thin slab with normal along [010]. The pump beam, of $\sim$2-W time averaged power focused to an $\sim$0.5-mm-diam spot, propagated along a direction just a few degrees removed from [010] and was polarized with electric field parallel to [001]. The signal beam propagated along [010] and was polarized either along [001] ("parallel" polarization) or along [100] ("perpendicular" polarization).

The resultant absorption spectra are shown in Fig. 9. Ground-state absorption bands appear at 1040, 720, 550, and 340 nm. (Meaningful studies could not be carried out for $\lambda \lesssim 300$ nm because of a high opacity of the samples in that region.) Unfortunately the 720-nm band is partially overlapped by a strong excited-state absorption signal, such that only the long-wavelength tail of the former is revealed; the dotted line shows a reconstruction of the full 720-nm band. The signals all showed the required $\sim 27°$ phase lag with respect to the pump modulation, except over a narrow region (650 nm $\lesssim \lambda \lesssim$ 700 nm) on the short-wavelength side of the 720-nm band. The signal amplitude also behaved erratically in this region, showing significant variation from sample to sample. This spurious behavior must be due to the presence of another species, also pumped by light at

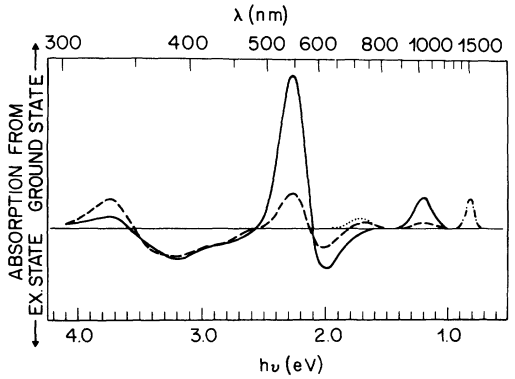

FIG. 9. Results of the tagged absorption measurement on the $Tl^0(1)$ center. The pump field E_p was parallel to [100]; both pump and observation beams propagated along [001]. Solid curve: $\vec{E}_{obs} \| [100]$. Dashed curve: $\vec{E}_{obs} \| [010]$. Dot-dash curve: luminescence. Dotted curve: Reconstruction of the 720-nm band.

1.06 μm, and having absorption in the region of difficulty.

It should be pointed out that virtually the same spectrum as that shown in Fig. 9 was obtained when the pump wavelength was 576 nm (from a krypton ion laser). Although it is more difficult to guarantee that energy transfer to other species will not take place for pumping at the shorter wavelength, the experiment is nevertheless useful as confirmation of results obtained with pumping in the fundamental band. To be able to pump at alternate wavelengths is also useful for filling in the region immediately surrounding the original pump wavelength. (Signals in that region are subject to interference from strong pump light.) In fact, Fig. 9 represents a composite of results from the two experiments, as the 1040-nm band displayed there was obtained from pumping with the shorter wavelength.

The ground-state absorption spectrum as revealed in Fig. 9 thus provides the vital verification that the 720- and 550-nm bands do indeed originate from the same center as the 1040-nm band. The spectrum also yields vital information about the polarizations and relative strengths of the bands. Once again there is very good agreement with theoretical prediction, as will be revealed more fully in the following section.

In examining the excited-state absorption, we have looked carefully down to energies as low as $\sim$4000 cm^{-1}. (Difficulties with sources and detectors forced us to abandon the search at lower energies.) Furthermore, on theoretical grounds, the energy of the lowest excited-state absorption ($\Psi_* \rightarrow \Sigma_*$) is expected to be *greater* than that (8565 cm^{-1}) between the same two states in the normal configuration. (See Fig. 10.) *Therefore, we are forced to conclude that the band peaking at $\sim$620 nm, as the lowest-energy excited-state absorption, must represent the $\Psi_* \rightarrow \Sigma_*$ transition.* It is a bit surprising that the transition energy ($\sim$16 130 cm^{-1}) is so much larger than the corresponding value (the 8565 cm^{-1} cited above) obtaining for the normal configuration. However, as we shall show in the next section, the polarization of the 620-nm band indicated in Fig. 9 fits rather well theoretical prediction for the $\Psi_* \rightarrow \Sigma_*$ transition.

Finally, it is tempting to associate the 340-nm band and the higher excited-state absorptions seen in Fig. 9 with transition to various components of the crystal-field split 6*d* level. To be sure, the total oscillator strength for the higher excited-state absorption bands (or groups of bands) is much smaller than the value (f = 0.28) obtaining in the free atom for the $6p\ ^2P_{3/2} \rightarrow 6d^2D_{3/2}$ transition. However, one probably can argue that the oscillator strength should be greatly reduced for transition to states that are either near to or degenerate with the continuum. Further discussion of transitions to the higher excited states is beyond the scope of this paper.

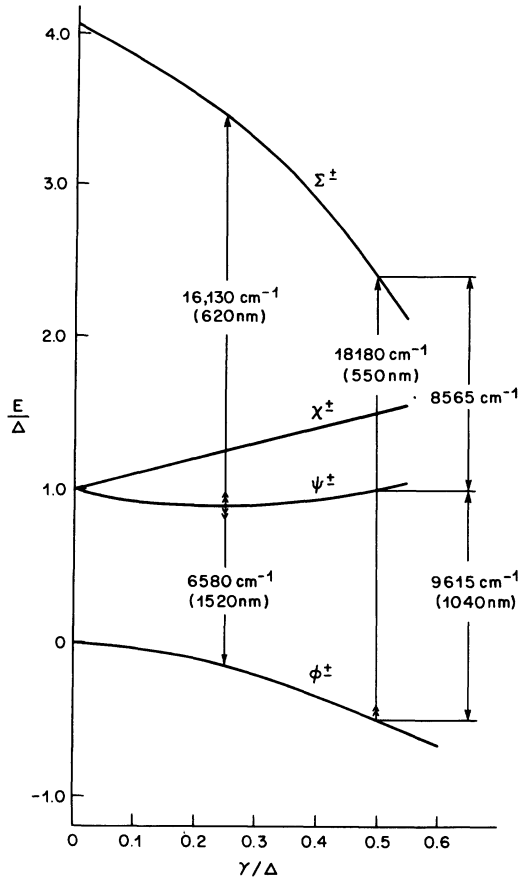

FIG. 10. Empirically determined behavior of the Σ-state energy, referred to energies of the 6*p* manifold. The curve of Σ-state energy is based on points at γ/Δ=0,0.25, and 0.5. The point at γ/Δ=0 reflects the $6P_{1/2} \rightarrow 7S$ transition energy of the free atom, while the other two points are based on the indicated transition energies for the relaxed and normal configurations, respectively, of the color center. (Note: As indicated earlier, the energy difference between the Σ state and the ground state depends on other crystal-field factors in addition to γ. Therefore, for the purposes of the above diagram, it should be understood that the other crystal-field components are considered to scale with γ, although they do not strictly do so in reality.)

E. Polarizations and relative strengths of the major transitions

As noted in the preceding section, the tagging experiment yielded much fundamental information concerning the polarizations of the detected transitions. However, in order to interpret the results, one must take into account the fact that the crystal con-

tains equal numbers of $Tl^0(1)$ centers with z axis parallel to each of the [001], [010], and [100] directions. The measured polarization ratios then represent a folding of various pumping rates with the polarization ratio intrinsic to the transition. To completely unscramble the data, more information is required. The desired information can be obtained from measurements of the emission polarization.

Therefore, we performed the experiment indicated in Fig. 11. An optically thin crystal slab (normal [010]) was pumped by the unfocused beam, propagating along [010] and polarized parallel to [001], of a cw laser beam of wavelength making essential match to either the 1040- or the 550-nm bands. The emission propagating along the [010] axis was then analyzed into "parallel" ($E||[001]$) and "perpendicular" ($E||[100]$) components. Let us designate the resultant intensities as $I_{||}$ and $I_\perp$, respectively. Let $\rho_1 \equiv I_{||}/I_\perp$, for pumping in the 1040-nm band, and $\rho_2 \equiv I_{||}/I_\perp$ for pumping in the 550-nm band. The experimental results were $\rho_1 = 3.0$ (see Fig. 12) and $\rho_2 = 5.2$.

For analysis of the tagging experiment, let $A_{||}$ and $A_\perp$ be absorption strengths analogous to the quantities $I_{||}$ and $I_\perp$. It should be noted that the ratio $A_{||}/A_\perp$ measured at 550 nm while pumping in the 1040-nm band should be (and essentially is) identical to $A_{||}/A_\perp$ measured at 1040 nm while pumping in the 550-nm band. Let us call the common ratio ρ_3. From Fig. 9, $\rho_3 = 5.0$. Finally, let the ratios σ_z/σ_x be designated R_1, R_2, and E, for the 1040-nm, 550-nm, and emission (1.52 μm) bands, respectively.

It can easily be shown that the measured ratios ρ_1, ρ_2, and ρ_3 are related to the quantities R_1, R_2, and E by the following equations:

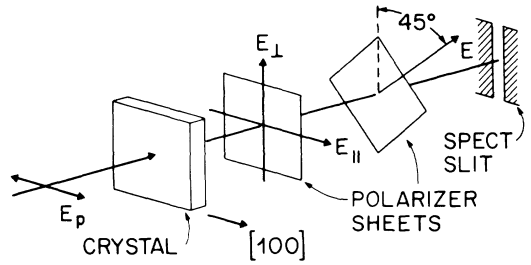

FIG. 11. Experimental arrangement for measuring polarization of the luminescence. The field of the pump, E_p, is polarized parallel to [100]. The first polarizer selects either $E_{||}$ or $E_\perp$ of the luminescence; the second polarizer selects equal representations of $E_{||}$ and $E_\perp$ along a common axis, in order to avoid effects of polarization preference by the spectrometer.

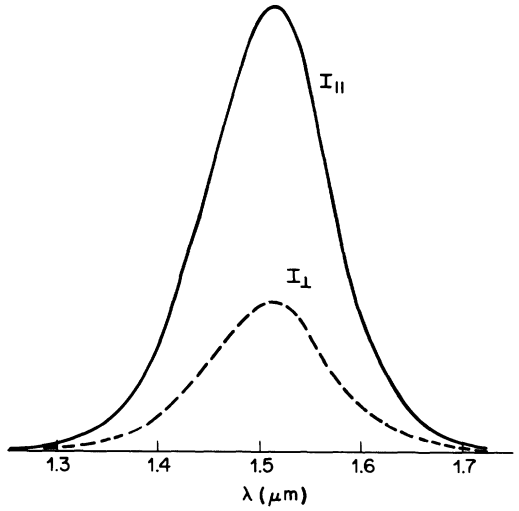

FIG. 12. Luminescence intensity of the $Tl^0(1)$ center vs wavelength for the "parallel" and "perpendicular" polarizations indicated in Fig. 11 and for pumping in the 1040-nm band.

$$\rho_1 = \frac{R_1 E + 2}{R_1 + E + 1}, \tag{14a}$$

$$\rho_2 = \frac{R_2 E + 2}{R_2 + E + 1}, \tag{14b}$$

$$\rho_3 = \frac{R_1 R_2 + 2}{R_1 + R_2 + 1}. \tag{14c}$$

The solution to the above equations, for the values of ρ_1, ρ_2, and ρ_3 cited, are summarized below in the bottom row (columns 1, 2, and 4) of Table III. Also included in the bottom row are the experimentally determined polarization ratios for the 720- and 620-nm bands; all that can be said about the former, in view of the experimental difficulties cited in the last section, is that it is quite small; the latter was derived from an equation similar to Eq. (14c), by using the already determined ratio R_1, and with R_2 now referring to the 620-nm band. The theoretical values in all but column 2 of Table III were obtained by taking $\epsilon = 0.317$, a value chosen such that the calculated polarization ratio (σ_z/σ_x) for the 1040-nm band would match the experimentally determined value (R_1). The parameter ϵ_* is probably somewhat smaller than ϵ, but it is not known by what factor. Therefore, where a value for ϵ_* was required (column 2) we have set ϵ_* also equal to 0.317. Note that the across-the-board agreement has been obtained with essentially one adjustable parameter (ϵ). (The quantity ϵ_* is not truly independent of ϵ, and in any event, it affects only one of the five ratios.)

The predicted relative intensities of the four ab-

TABLE III. Theoretical cross sections and polarization ratios for $\epsilon=0.317$. Abs. means absorption and Em. emission.

Transition →	$\Phi\rightarrow\Psi$ (Abs. at 1040 nm)	$\Psi^*\rightarrow\Phi^*$ (Em. at 1520 nm)	$\Phi\rightarrow\chi$ (Abs. at 720 nm)	$\Phi\rightarrow\Sigma$ (Abs. at 550 nm)	$\Phi^*\rightarrow\Sigma^*$ (Ex. state Abs. at 620 nm)
σ_z/σ_0 (Calc.)	$7.2\beta^2$	$7.0\beta^2$	0	3.26	1.63
σ_x/σ_0 (Calc.)	$1.2\beta^2$	$1.23\beta^2$	$1.1\beta^2$	0.017	0.66
σ_z/σ_x (Calc.)	6.0[a]	5.7	0	171	2.46
σ_z/σ_x (Expt.)	6.0	6.3	~0	32	3.0

[a]Adjusted to match the experimental value. See text.

sorptions (of Table III) can also be compared with experiment. From Fig. 9, the ratio of 550- to 1040-nm-band intensities (z polarization) is 6.6; by setting the theoretical ratio equal to that experimental value, one obtains $\beta^2=0.0686$ or $\beta=0.26$. (This value of β is just barely small enough to justify our use of a perturbation calculation for the mixing of Σ states with the $6p$ manifold.) The other two ratios, shown below in Table IV can then be calculated. (Note that there are only three independent ratios among the four absorption intensities.)

Once again, the agreement between theory and experiment is truly amazing, especially when one realizes that precise comparison involves several difficulties. First, for reasons cited earlier, the experimental intensity for the 720-nm band is somewhat uncertain. With respect to the 620-nm band, there are two uncertainties: (1) The (weaker) 620-nm band is partially overlapped by the 550-nm band, thereby making the former appear relatively less strong than it really is. (No attempt has been made to completely resolve the two bands.) (2) The calculated intensities for the 620- and 550-nm bands can be compared on an equal basis only on the (probably incorrect) assumption that relaxation makes no changes in the radial parts of the wave functions, and hence in the radial parts of the transition matrix elements.

Finally, we note that if, as indicated earlier (Sec. III C) the oscillator strength of the 1040-nm band is on the order of 2 to 4 times as great as that measured ($f = 0.0075$) for the luminescence band, then the oscillator strength for the 550-μm band lies somewhere between the limits ~0.1 and ~0.2. Note that the oscillator strength for the (approximately) corresponding transition in atomic Tl ($6^2P_{1/2}\rightarrow 7^2S_{1/2}$) is $f\cong 0.15$.

To sum up, the agreement between theory and experiment, with respect to polarization and band strengths for transitions of the $6p$-Σ state manifold, is essentially complete. It is hard to believe that such extensive agreement could be entirely fortuitous. Hence the agreement forms one of the strongest arguments in favor of our simple $Tl^0(1)$ model.

TABLE IV. Relative band intensities.

Transitions	550 nm(σ_z) / 1040 nm(σ_z)	720 nm(σ_x) / 1040 nm(σ_z)	620 nm(σ_z) / 550 nm(σ_z)
Intensity ratio (Calc.)	6.6[a]	0.15	~0.49
Intensity ratio (Expt.)	6.6	~0.25	~0.3

[a]Adjusted to match the experimental value. See text.

IV. SUMMARY AND CONCLUSION

By means of simple, tagged absorption spectroscopy in radiation-damaged KCl:Tl, we have identified three additional ground-state absorption bands belonging to the laser active center whose fundamental absorption peaks at 1040 nm. We have found only one emission band (the previously discovered laser band) definitely associated with that center. In addition to the band energies, we have measured oscillator strengths and polarization properties for all five transitions.

We have investigated the model of a neutral Tl atom with an adjacent anion vacancy, or the $Tl^0(1)$ model originated by Goovaerts *et al.* (Ref. 1) to explain the ground-state ESR. In particular, we have extended that model to calculate energies and wave functions for excited states of the $6p$ manifold. We have also been able to create a semiempirical model of the first even-parity (Σ) state.

We have found that predictions of the simple $Tl^0(1)$ model make a remarkable and extensive fit to our optical data. First, with just two adjustable parameters (the crystal-field energy γ and the spin-orbit splitting Δ, the latter only slightly adjustable),

measured transition energies of the $6p$ manifold (including the Stokes shift between absorption and emission of the fundamental transition) can be fitted to within a few percent. Second, with adjustment of only two other parameters (the wave-function admixture coefficients β and ϵ), we can fit the measured polarization and relative strengths of five principal transitions (the first three absorptions from the ground state, the lowest-energy absorption from the first excited state, and the emission). The most outstanding features of that agreement are as follows: (1) The 550-nm band is strongly z polarized and has a high oscillator strength because it represents transition from an orbital of largely p_z character to a largely s-like (Σ) state. (2) The much weaker 720-nm band is polarized in the xy plane because it represents transition from a small Σ component of the ground state to a pure p_{xy} orbital. (3) The 1040-nm band and associated emission band involve small Σ-state admixture in both initial and final states; their (z) polarizations, which would otherwise be rather modest, are considerably enhanced by the fact that the Σ state is somewhat elongated along the z axis, due to a substantial admixture of $|2,0\rangle$ state with the major $|0,0\rangle$ component.

Perhaps it should be explicitly stated that the data of this work will not support an F_A-center model, i.e., the model of an F center perturbed by a nearest-neighbor Tl^+ ion. Such a model requires an essentially s-like ground state, in contrast to the p-like ground state found here and in Ref. 1. Then the relatively low measured oscillator strengths of the two lowest-energy transitions (the 1040- and 720-nm bands) would require that the first two excited states also be largely s-like. However, such a succession of states is quite unlikely. Also, of course, one would be hard put to explain the polarizations measured here.

Finally, it should be noted that the $Tl^0(1)$ model is consistent with the observed high stability of the center, both on the shelf and in use as a laser gain medium. First, as an entity electrically neutral with respect to the surrounding crystal, the $Tl^0(1)$ center should be at most only a very shallow electron trap; thus a trapped electron should be easily and quickly removed by the laser pump light. Second, as pointed out earlier in Sec. III A, the two components of the $Tl^0(1)$ center should exert a Coulomb attraction for each other. For unit charges separated by the cation-anion distance (3.15 Å) in KCl, the attractive potential is about 4.5 V; however "delocalization" of the center's electronic charge (away from the Tl atom) may reduce this potential somewhat. Nevertheless, a Coulomb term of at least 1 V is to be expected, and this is to be added to all the other energies required for breakup of the center. Thus, the total binding energy of the $Tl^0(1)$ center should be considerably greater than the $\sim$1-V binding energies of the known F_A centers.

ACKNOWLEDGMENTS

We would like to thank Professor R. Bartram for a helpful discussion. One of us (N. Vieira) would like to thank the Brazilian Nuclear Energy Commission (C.N.E.N.) for a scholarship.

APPENDIX A: DETAILS OF CALCULATION OF THE RELATIVE Σ-STATE ADMIXTURES INTO STATES OF THE $6p$ MANIFOLD

As already noted in the text, the coefficients of Σ-state admixture into various states of the $6p$ manifold involve matrix elements of $V_1(\vec{r})$. Since $V_1(\vec{r})$ has a $|1,0\rangle$ angular dependence, the desired matrix elements are proportional to a weighted sum of the coefficient of the $|1,0\rangle$ terms of the involved p-like state ($\Phi^{\pm}$ or $\Psi^{\pm}$), and where the weighting is in proportion to matrix elements of the radial part $[a(r)]$ of $V_1(\vec{r})$.

We have approximated the matrix elements of $a(r)$ by the matrix elements of r. (For a table of the latter, see Appendix B.) At first the approximation may seem a bit gross, since $a(r)$ is proportional to r only for $r<r_0$. However, the absolute error in weighting factors is really not all that great. For example, consider the matrix elements connecting $6P$ states to the $7S$ state. To ignore altogether the difference in radial dependencies of the $6p^2P_{3/2}$ and $6p^2P_{1/2}$ states leads to a relative weighting factor of 1, whereas use of the relative matrix elements of r leads to a weighting factor of $\sqrt{1.6}=1.26$ in favor of coefficients of the $P_{3/2}$ state. The former approximation underestimates the true ratio, while the latter overestimates it. Thus the true ratio is at least bracketed by those two limits. However, a crude numerical integration indicates that the true ratio lies considerably closer to the higher limit than to unity.

To further simplify matters, we have temporarily set ϵ (the coefficient of the $|2,0\rangle$ component to Σ) equal to zero, since ϵ is not known until calculated optical properties (strongly dependent on the relation Σ-state admixtures) have been compared with the results of experiment. However, we have discovered that inclusion of the empirically determined ϵ leads to no significant change (less than 1%) in the relative Σ-state admixture into the Φ and Ψ states.

Thus, to illustrate, the relative coefficient of Σ^+ mixed into the Ψ^+ state was calculated as

$$(0.819\sqrt{2/3}\sqrt{1.6}-0.574\sqrt{1/3})/0.472=1.09\ ,$$

whereas the corresponding quantity for the Φ^+ state was calculated as

$$(-0.819\sqrt{1/3}-0.574\sqrt{1.6}\sqrt{2/3})/1=-1.066\ ,$$

where the quantities 0.472 and 1 represent the relative energy denominators. The ratio of the two relative coefficients (there is no meaning to their absolute values) is (by accident) essentially -1, just as indicated in Eqs. (7a) and (7b).

APPENDIX B: ELEMENTS OF TRANSITION MATRICES

Angular integrals for $s\rightarrow p$ and $p\rightarrow d$ transitions[10] where

$$I^+\equiv\sqrt{4\pi/3}\langle l',m' \mid 1,m'-m \mid l,m\rangle(l\rightarrow l+1)\ ,$$

$$I^-\equiv\sqrt{4\pi/3}\langle l,m \mid l,m-m' \mid l',m'\rangle(l'\rightarrow l'-1)\ ,$$

and

$$I_0\equiv\sqrt{4\pi/3}\langle 0,0 \mid 1,0 \mid 1,0\rangle\ .$$

l,l'	m	m'	$I^{\pm}$	$I^{\pm}/I_0$
	0	±1	$\pm\sqrt{1/3}$	±1
0,1	0	0	$\sqrt{1/3}$	1
	±1	±2	$\pm\sqrt{6/15}$	$\pm\sqrt{6/5}$
	±1	±1	$\sqrt{3/15}$	$\sqrt{3/5}$
1,2	±1	0	$\pm\sqrt{1/15}$	$\pm\sqrt{1/5}$
	0	±1	$\pm\sqrt{3/15}$	$\pm\sqrt{3/5}$
	0	0	$\sqrt{4/15}$	$\sqrt{4/5}$

Radial integrals $f(ba)=(2m\omega_{ab}/9\hbar)\xi\,|R_{ab}|^2$, where $R_{ab}=\langle r\rangle_{ab}$.

Transition $a\rightarrow b$	ξ	$\tilde{\nu}_{ab}$ (cm^{-1})	f From Expt. (Ref. 11)	$\frac{R_{ab}}{R(P_{1/2}\rightarrow S_{1/2})}$ From Calc. (Ref. 6)	From f_{expt}
$6^2P_{1/2}\rightarrow7^2S_{1/2}$	1	26477	0.133	1	1
$6^2P_{3/2}\rightarrow7^2S_{1/2}$	1	18684	0.151	$\sqrt{2.03}$	$\sqrt{1.60}$
$6^2P_{1/2}\rightarrow6^2D_{3/2}$	2	36118	0.29	$-\sqrt{1.09}$	$-\sqrt{0.80}$
$6^2P_{3/2}\rightarrow6^2D_{5/2}$	$\frac{9}{5}$	28407	0.346	$-\sqrt{2.04}$	$-\sqrt{1.34}$
$6^2P_{3/2}\rightarrow6^2D_{3/2}$	$\frac{1}{5}$	28325	0.040	$-\sqrt{2.03}$	$-\sqrt{1.40}$

*Visitor, Instituto de Penquisas Energeticas e Nucleares, São Paulo, Brazil.

[1]E. Goovaerts, J. Andriessen, S. V. Nistor, and D. Schoemaker, Phys. Rev. B 24, 29 (1981). Also see P. G. Baranov and V. A. Khramtsov, Phys. Stat. Sol. (b) 101, 153 (1980).

[2]W. Gellerman, F. Luty and C. R. Pollock, Optics Comm. 39, 391 (1981).

[3]C. J. Delbecq, A. K. Ghosh, and P. H. Yuster, Phys. Rev. 151, 599 (1966).

[4]C. J. Delbecq, A. K. Ghosh, and P. H. Yuster, Phys. Rev. 154, 797 (1967).

[5]R. S. Knox, Phys. Rev. 154, 799 (1967).

[6]D. V. Neuffer and E. D. Commins, Phys. Rev. A 16, 844 (1977).

[7]C. J. Delbecq, Y. Toyozawa, and P. H. Yuster, Phys. Rev. 9, 4497 (1974).

[8]D. S. McClure, *Electronic Spectra of Molecules and Ions in Crystals*, Solid State Physics, Vol. 9, edited by F. Seitz and D. Turnbull (Academic, New York, 1959).

[9]L. F. Mollenauer, Phys. Rev. Lett. 43, 1524 (1979).

[10]From Table 11.1, p. 246 of M. Weissbluth, *Atoms and Molecules* (Academic, New York, 1978). This is an excellent general reference for theory, with many useful tables containing Clebsch-Gordan coefficients, elementary wave functions, various matrix elements, etc.

[11]A. Gallagher and A. Lurin, Phys. Rev. A 136, 87 (1964).